Check for updates

Noncovalent binding phenomena in the adsorption of amino acids on Ag/Au surfaces: a theoretical approach†

Catalina Nicolau, Sergi Burguera, [ID] María de las Nieves Piña [ID] and Antonio Bauzá [ID] *

Adsorption of amino acids (AAs) onto Ag and Au surfaces has attracted much interest in the past years, owing to their ability to control and tune the structure of Ag and Au nanoparticles (NPs) during the synthetic procedure and to enhance their stability under various conditions. Despite this, the molecular recognition events that are responsible for such stabilization as well as the role of the AA residue moieties is still not completely understood. To tackle this point, we computationally evaluated the weak interactions involved in the AA···Ag/AuNP recognition process from a theoretical perspective. In more detail, we analysed the strength and physical nature of the interactions established between twenty essential AAs and Ag/AuNPs at the PBE0-D3/def2-TZVP level of theory. The structural and energetic studies were complemented by the use of the quantum theory of atoms in molecules (QTAIM), non-covalent interaction plot (NCIplot) and energy decomposition analysis (EDA) techniques, providing new insights into the nature and spatial extension of the interactions studied herein. We believe that the results reported in this exploratory study will be useful for researchers working in the fields of bioinorganic chemistry, biotechnology and supramolecular chemistry by shedding light on the weak binding phenomena that are crucial for achieving AA···Ag/AuNP recognition.

Introduction

Nanotechnology has revolutionized various scientific disciplines, particularly in the fields of medicine,[1] materials science,[2] and biochemistry.[3] Among the vast number of nanomaterials studied, silver and gold nanoparticles (AgNPs and AuNPs) have attracted significant attention in recent years due to their unique physico-chemical properties, including their high surface area-to-volume ratio, tunable optical properties, and remarkable biocompatibility,[4] exhibiting immense potential for application in various fields ranging from drug delivery and biosensing[5] to antimicrobial treatment and cancer therapy.[6]

A crucial aspect of their functionality in biological systems is their interaction with biomolecules, particularly peptides, proteins, and amino acids (AAs),[7] for instance, for controlling the structure of Ag/AuNPs during synthesis and improve their stability under various conditions.[8] In this context, studies have demonstrated that the binding affinity of a given peptide for a particular region of the metal surface is related to the peptide's ability to control nanoparticle synthesis and enhance stability.[9,10]

Peptides, proteins, and AAs exhibit a diverse range of interactions with metallic nanoparticles, influenced by factors such as nanoparticle size, shape, surface charge, and functionalization, as well as the intrinsic properties of the biomolecules themselves.[11] These interactions can lead to the formation of stable protein coronas,[12] affect protein conformational stability,[13] and influence cellular uptake and biological responses.[14] In fact, the ability of AAs to bind to metal surfaces through functional groups such as thiols, amines, and carboxyls plays a pivotal role in modulating nanoparticle behavior and stability.[15] In this regard, previous experimental and computational studies have delved into the atomic-level details of binding between peptides and Ag surfaces.[16,17] However, the nature of the interactions governing the AA···NP molecular recognition mechanism is not completely understood, and its study is essential for designing novel NPs for specific biomedical applications (*e.g.* to increase therapeutic efficacy or to improve targeting specificity in drug delivery systems).

This study aims to explore the noncovalent interactions (NCIs) between AAs and Ag/AuNPs from a theoretical perspective. To achieve this, we have used twenty natural AAs and a model of Ag/AuNPs (see Fig. 1 and the Methods section). In more detail, we have computationally simulated the

Ctra. de Valldemossa, km. 7.5, Universitat de les Illes Balears, 07122, Palma de Mallorca, Islas Baleares, Spain. E-mail: antonio.bauzaatuib.es

† Electronic supplementary information (ESI) available. See DOI: https://doi.org/10.1039/d5cp01106j

This journal is © the Owner Societies 2025

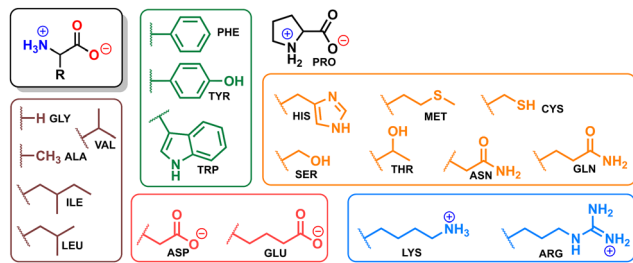*Phys. Chem. Chem. Phys.*, 2025, **27**, 9463–9469 | **9463**

Fig. 1 Schematic representation of the AAs used in this study (brown = non-polar, green = aromatic, red and blue = polar charged, orange = polar neutral).

supramolecular complexes formed when the AAs are adsorbed onto the metallic surface, leading to the characterization of the NCIs responsible for this process. The supramolecular assemblies found were further studied using quantum mechanical techniques including the molecular electrostatic potential (MEP), the quantum theory of atoms in molecules (QTAIM), the non-covalent interaction plot (NCIplot) and the energy decomposition analysis (EDA) methodologies.

Methods

The interaction energies of all complexes included in this study were computed at the PBE0[18,19]-D3[20]/def2-TZVP[21] level of theory. The calculations were performed using the program TURBOMOLE version 7.7.[22] Concretely, the Ag and Au layers were built using the geometries retrieved from the study of Sawabe and collaborators,[23] by utilizing a moiety of 26 atoms belonging to the 282-atom cluster (which belongs to one of the "faces" of the metal decahedron structure). The metal layer was kept

frozen, while the AA was left freely to explore the most favourable disposition. The conductor like screening model for real solvents (COSMO-RS)[24] was used within the TURBOMOLE 7.7. framework during the calculations using water as a solvent. The interaction energies were calculated using the supermolecule approximation ($\Delta E = E_{Ag/Au\ layer-AA\ complex} - E_{AA} - E_{Ag/Au\ layer}$). The optimizations were carried out without imposing symmetry on the system. The initial disposition of AA over the metallic layer was set to be with the carboxylate group of the zwitterion moiety pointing outwards, to not overestimate the energetic results. This group is also supposed to be solvated and not involved in the formation of the AA···NP supramolecular complex. The optimized structures do not correspond to fully relaxed geometries since we wanted to preserve the original geometry of the metal layer when extracted from the cluster, and therefore frequency analysis calculations were not performed.

The MEP surfaces were computed at the PBE0-D3/def2-TZVP level of theory using the Gaussian 16 software[25] and analyzed using the GaussView 5.0 program.[26] The calculations for the wavefunction analysis[27] were also carried out at the PBE0-D3/def2-TZVP level of theory and analyzed using the AIMAll software.[28]

In addition, the energy decomposition analysis (EDA)[29,30] scheme was used to understand the role of electrostatics, exchange-repulsion, orbital, dispersion and electron correlation contributions in the formation of the noncovalent complexes studied herein at the PBE0-D3/def2-TZVP level of theory using TURBOMOLE 7.7 software and the COSMO-RS approximation.

Lastly, the NCIplot[31] isosurfaces correspond to both favorable and unfavorable interactions, as differentiated by the sign
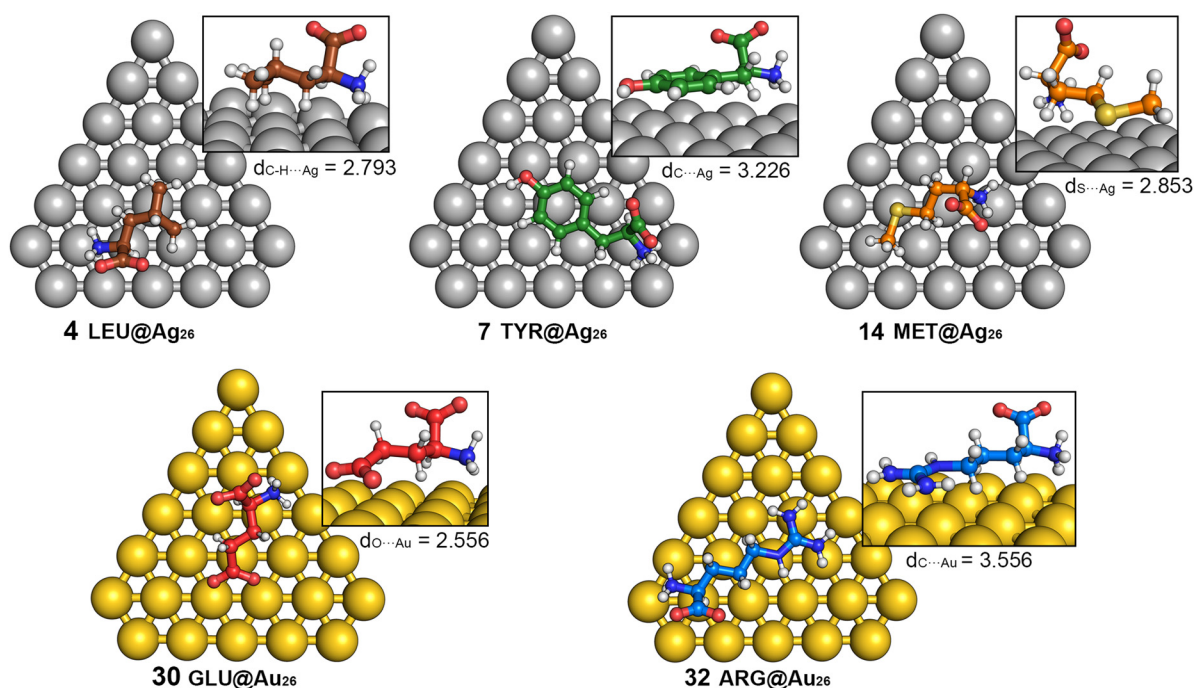

Fig. 2 Optimized geometries at the PBE0–D3/def2–TZVP level of theory of complexes **4**, **7**, **14**, **30** and **32**. The AA···Ag26/Au26 distance is also given in Å.

9464 | *Phys. Chem. Chem. Phys.*, 2025, **27**, 9463–9469

This journal is © the Owner Societies 2025

of the second-density Hessian eigenvalue and defined by the isosurface color. The color scheme is a red–yellow–green–blue scale, with red indicating repulsive (ρ_{cut}^+) and blue indicating attractive (ρ_{cut}^-) NCI interaction densities. Yellow and green surfaces correspond to weak repulsive and weak attractive interactions, respectively. The surfaces were visualized using the Visual Molecular Dynamics (VMD) software.[32]

Results and discussion

Structural and energetic features of the AA···NP recognition

Fig. 2 and Table 1 presents the results from calculations for complexes **1–20** involving Ag26 and complexes **21–40** involving Au26. As noted, for both sets of complexes, attractive interaction energy values were found, ranging between −18.7 and −3.8 kcal mol^{-1} in the case of Ag-involving complexes and

Table 1 Interaction energy values (ΔE, in kcal mol^{-1}), equilibrium distances (d, in Å) and distance/sum of the vdW radii ratio (d/∑ vdW), including the interacting amino acid (AA) for Ag and Au complexes **1–40** at the PBE0-D3/def2-TZVP level of theory

Complex	AA	ΔE	d	d/∑ vdW
AA···Ag complexes				
1	GLY	−3.8	2.787	0.75
2	ALA	−4.4	3.142	0.84
3	VAL	−8.0	2.528	0.68
4	LEU	−9.5	2.793	0.75
5	ILE	−9.9	2.701	0.72
6	PHE	−18.2	3.039	0.71
7	TYR	−18.7	3.098	0.77
8	TRP	−18.6	2.995	0.70
9	ASP	−14.6	2.721	0.68
10	GLU	−9.5	2.593	0.64
11	LYS	−6.5	2.829	0.76
12	ARG	−13.0	3.610	0.84
13	HIS	−13.5	3.048	0.73
14	MET	−13.7	2.853	0.65
15	CYS	−10.0	3.115	0.70
16	SER	−10.6	3.278	0.81
17	THR	−5.8	3.022	0.75
18	ASN	−7.2	2.855	0.71
19	GLN	−10.6	2.884	0.72
20	PRO	−7.4	2.882	0.78
AA···Au complexes				
21	GLY	−5.7	2.673	0.73
22	ALA	−6.3	3.118	0.85
23	VAL	−11.5	2.484	0.68
24	LEU	−13.1	2.771	0.76
25	ILE	−13.5	2.645	0.72
26	PHE	−24.8	2.959	0.70
27	TYR	−25.6	3.135	0.79
28	TRP	−27.6	3.006	0.71
29	ASP	−18.5	2.564	0.70
30	GLU	−14.1	2.556	0.65
31	LYS	−10.4	2.802	0.77
32	ARG	−17.9	3.557	0.84
33	HIS	−18.6	3.025	0.74
34	MET	−21.3	2.675	0.62
35	CYS	−13.5	2.994	0.69
36	SER	−11.3	3.299	0.84
37	THR	−6.5	3.312	0.84
38	ASN	−10.2	3.011	0.76
39	GLN	−14.6	3.001	0.76
40	PRO	−10.5	2.881	0.79

between −27.6 and −5.7 kcal mol^{-1} in the case of Au-involving complexes, which achieved more favourable interaction energy values in all the cases. Furthermore, as it can be observed from Fig. 2, for most of the computed supramolecular complexes (except for complexes **9** and **29**), it is the AA residue that makes the most intermolecular contacts between both entities, and thus the interaction energies obtained are closely related to the size and electronic nature of the residues involved.

Firstly, from complexes **1** and **21** (GLY) to complexes **5** and **25** (ILE), we observed a progressive reinforcement of the interaction energy value, in line with the increase in the extension of the AA residue. These aliphatic AAs based their interaction with the metallic surface on CH–Rg (Rg = Ag and Au) contacts, similarly to the results obtained in our previous study involving aryl substituted aromatic VOCs.[33] These NCIs can also be understood as hydrogen bonds (HBs), since the electrostatic potential surface of the metallic layers exhibits both positive (holes) and negative (lumps) regions, thus being able to act as both an electron donor and an acceptor moiety (see Fig. 3).

Secondly, for complexes **6–8** and **26–28** (PHE, TYR and TRP), the interaction energy values obtained were similar in the case of Ag26 (−18.2, −18.7 and −18.6 kcal mol^{-1}, respectively), while more noticeable energetic differences were found among the Au26-involving complexes (−24.8, −25.6 and −27.6 kcal mol^{-1}, respectively). In both sets, we observed a strengthening of the interaction from PHE to TYR owing to the alcohol group that establishes an additional regium bond (RgB)[34–39] with the metallic layer (see also Fig. 4a and b). However, we found that in the case of Ag26, complex **8** involving TRP achieved a very similar value to complex **7** involving TYR, while in the case of
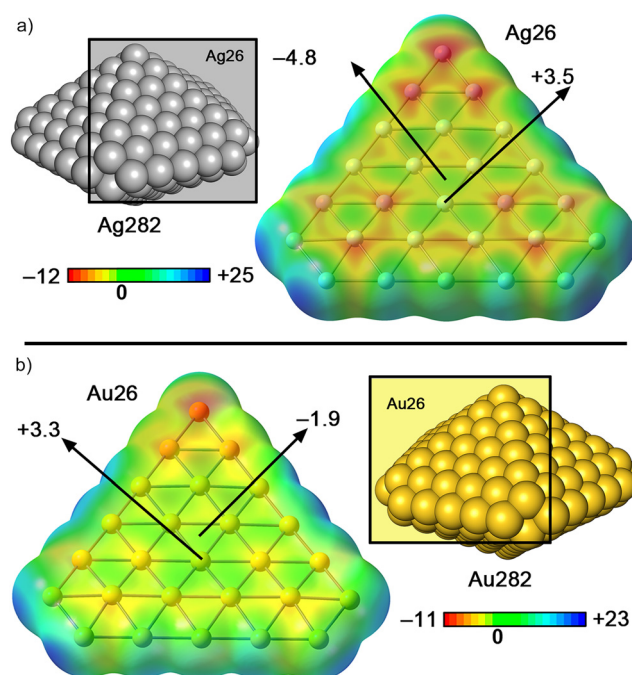

Fig. 3 MEP surfaces of Ag26 (a) and Au26 (b) layers. The energy values at concrete parts of the surface are given in kcal mol^{-1} (0.002 a.u.).
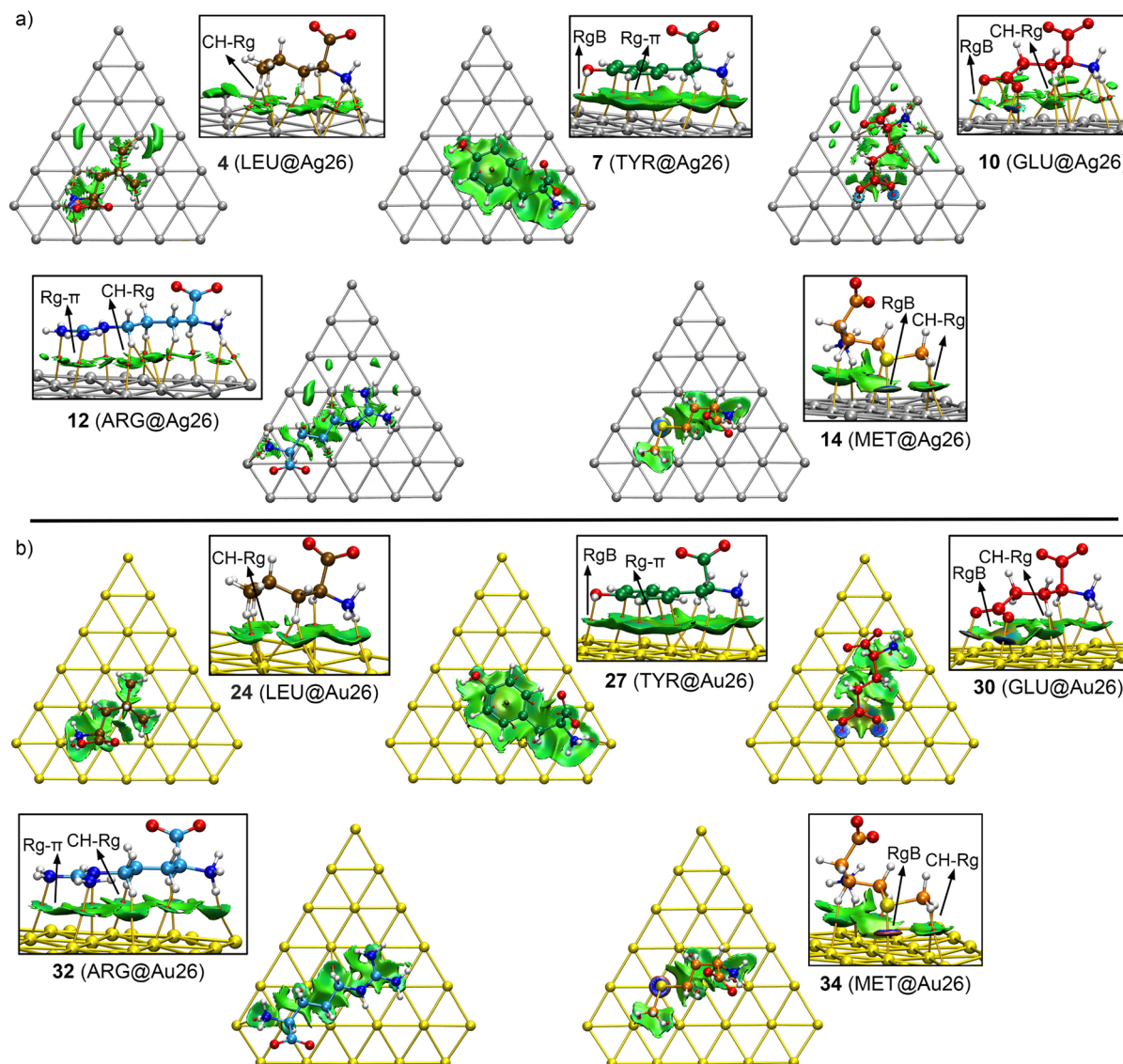
Fig. 4 NCIplot analysis and QTAIM distribution of intermolecular bond critical points (bcps in red spheres) and bond paths in complexes **4**, **7**, **10**, **12** and **14** involving Ag (a) and **24**, **27**, **30**, **32** and **34** involving Au (b). The names of the NCIs involved in the AA···Ag/AuNP recognition are indicated inside the square parts of the figure. NCIplot surfaces only include intermolecular contacts between the AA and the NP. NCIplot colour range: -0.04 a.u. $\leq$ $(\text{sign}\,\lambda_2)\rho$ $\leq$ $+0.04$ a.u. Isosurface value (RDG) = 0.5 and ρ cutoff = 0.05 a.u.

Au26 we obtained an increase of 2 kcal mol^{-1} in stability, which is likely due to the higher stability exhibited by Au Rg–π bonds involving extended aromatic systems.[40]

For complexes involving charged AAs, that is, **9–12** and **29–32** (ASP, GLU, LYS and ARG), we also observed the same behaviour comparing the Ag26 with the Au26 series. Concretely, complexes involving ASP (**9** and **29**) and ARG (**12** and **32**) achieved higher interaction energy values than those involving GLU (**10** and **30**) and LYS (**11** and **31**). This is likely due to a larger contact area in the case of ARG-involving complexes owing to the presence of the guanidinium group, while between ASP and GLU, the latter showed the interaction of both carboxylate groups with the metal layer, thus partly overestimating the interaction energy value obtained.

Lastly, among the polar and neutral AAs (complexes **13–20** and **33–40**), several interesting points are worth discussing. For instance, between the two S-containing AAs (MET and CYS), a larger interaction energy value was obtained for complexes **14** (-13.7 kcal mol^{-1}) and **34** (-21.3 kcal mol^{-1}) involving the former, owing to its slightly higher basicity (in line with the shorter MET···NP distances). On the other hand, among the O-containing AAs (SER, THR, ASN and GLN), SER complexes (**16** and **36**) and GLN complexes (**19** and **39**) obtained the largest interaction energy values (-10.6 and -11.3 kcal mol^{-1} and -10.6 and -14.6 kcal mol^{-1}), owing to the formation of moderately strong O···Ag/Au RgBs. Furthermore, ASN complexes (**18** and **38**) obtained lower interaction energy values (-7.2 and -10.2 kcal mol^{-1}) compared to those involving GLN,

9466 | *Phys. Chem. Chem. Phys.*, 2025, **27**, 9463–9469

This journal is © the Owner Societies 2025

likely due to the shorter aliphatic chain present in the former. Moreover, HIS complexes (**13** and **33**) and PRO complexes (**20** and **40**) also exhibited moderately strong Rg–π and CH–Rg interactions, being HIS complexes more stable than their PRO analogues by around 6–8 kcal mol^{-1}.

Since most of the molecular recognition events occur due to a charge complementarity between the electron donor and acceptor molecules, we have computed the electrostatic potential surfaces of the two metallic layers used herein, Ag26 and Au26. As noted in Fig. 3, we found positive electrostatic potential regions (located over the Ag and Au atoms), which accounted for the presence of holes, and also negative potential regions (located in between the metal atoms), confirming the presence of lumps. These positive and negative potential regions allowed the metal layers to favorably interact with both electron-rich and electron-poor AA residues from an electrostatic point of view. Also, the MEP value over the holes is similar for both metal clusters (+3.5 kcal mol^{-1} in Ag26 and +3.3 kcal mol^{-1} in Au26), while the lumps present in the Ag26 cluster exhibited a more negative potential (-4.8 kcal mol^{-1}) compared to the Au26 cluster (-1.9 kcal mol^{-1}). In general, although the positive and negative electrostatic potential values obtained for both metal surfaces are useful to understand the role of electrostatics, the slight differences observed in the MEP values are not sufficient to completely rationalize the interaction energy values obtained; therefore, an energy decomposition study was also performed to further understand these energetic results (see below).

Analysing the physical nature of AA···NP contacts using QTAIM and NCIplot techniques

We have also explored the AA···NP interactions from a charge density perspective by conducting the QTAIM and NCIplot analyses (see Fig. 4 and Table 2) of a series of representative complexes (see Table S1, ESI,† for the data regarding the rest of the complexes).

As shown in Fig. 4, for complexes **4** and **24** involving LEU, the interaction between the AA and the metallic layer is characterized by the presence of several bond critical points (bcps) and bond paths connecting the alkyl group of LEU to the Ag/Au layer, thus confirming the presence of CH–Rg (Rg = Ag and Au) contacts. For complexes **7** and **27** involving TYR, the bcps and bond paths mainly connect the C atoms from the aromatic ring with the Ag/Au atoms from the metallic layer, thus characterizing these complexes as Rg–π bonds. In addition, the O atom from the alcohol group also shows a bcp and a bond path that connects it to a metal atom, thus also contributing to the overall stabilization of these complexes through the formation of a O···Rg RgB.

For complexes **10**, **12**, **30** and **32** involving GLU and ARG residues, several bcps and bond paths denote the presence of (i) CH–Rg interactions, (ii) RgBs, with the electron donor moiety being the AA in the case of complexes **10** and **12**, and (iii) Rg–π interactions in the case of complexes **30** and **32**. The CH–Rg contacts are characterized by the presence of bcps and bond paths connecting the CH bonds and the metal atoms, while

Table 2 Values of the density at the bond critical points ($\rho \times 100$, in a.u.) that characterize the NCIs present in complexes **4**, **7**, **10**, **12**, **14**, **24**, **27**, **30**, **32** and **34**, along with the values of the Laplacian of ρ ($\nabla^2\rho \times 100$) and the potential ($V \times 100$), kinetic ($G \times 100$) and total energy densities ($H \times 100$) as well as the $-G/V$ ratio given in a.u.

Complex[a]	$\rho \times 100$	$\nabla^2\rho \times 100$	$V \times 100$	$G \times 100$	$H \times 100$	$-G/V$
4	0.61	2.32	−0.53	0.56	0.03	1.06
7	1.06	3.81	−0.72	0.84	0.12	1.17
10	2.85	11.25	−3.20	3.01	−0.19	0.94
12	0.80	3.04	−0.72	0.74	0.02	1.03
14	3.26	8.17	−2.77	2.40	0.13	0.87
24	1.15	2.94	−0.63	0.68	0.05	1.08
27	1.17	4.26	−0.83	0.95	0.08	1.14
30	3.68	13.19	−3.60	3.45	−0.15	0.96
32	1.16	3.48	−0.74	0.81	0.07	1.09
34	5.31	11.57	−4.69	3.79	−0.90	0.81

[a] Only the bcps exhibiting the largest density values were considered.

RgBs and Rg–π interactions are denoted by O···Rg and N···Rg bcps and bond paths that involve either the carboxylate group or the guanidinium group of the AA and the metal layer.

Lastly, for complexes **14** and **34** involving MET, very similar bcp and bond path distribution were observed, including the presence of CH–Rg bcps and bond paths as well as a S···Rg bcp and a bond path that characterizes the presence of a RgB.

On the other hand, regarding the NCIplot analyses, in all the complexes a greenish isosurface was found, located between the AA and the metallic layer, which denotes the presence of weak but attractive NCIs. Additionally, in the case of the O···Rg and S···Rg interactions present in complexes **10**, **14**, **30** and **34**, a more bluish isosurface colour was observed, thus indicating the presence of a stronger interaction that likely dictates the molecular recognition event between both counterparts.

Table 2 presents the values of the Laplacian at the bcps that characterize the AA···NP interaction ($\nabla^2\rho \times 100$), resulting in positive values in all cases, as it is common in closed shell calculations. Furthermore, the values of the potential ($V \times 100$) and kinetic ($G \times 100$) energy densities lie within the same range in all the cases, leading to $-G/V$ ratios around 1, which confirm the noncovalent nature of the AA···NP interactions.

An EDA study to reveal the energetic contributions responsible for the AA···NP recognition

As the final stage of our research, we have performed an EDA study on the supramolecular complexes shown above. Five representative examples involving AAs of different nature (charged, aromatic, aliphatic and neutral) are included in Fig. 5 (see Table S2 and Fig. S1, S2, ESI,† for the rest of the complexes). The used energy partition scheme unveiled the contribution of electrostatics (Ele), exchange-repulsion (Ex-rep), orbital (Orb), dispersion (Disp), and electron correlation (Cor) terms.

As noted, in the case of the Ag26 layer, the dispersion term was the most noticeable contributor in the case of complexes involving ARG (**12**), TYR (**7**) and LEU (**4**), followed by correlation and orbital terms, which exhibited very similar values, and lastly electrostatics being the least favorable contributor to the
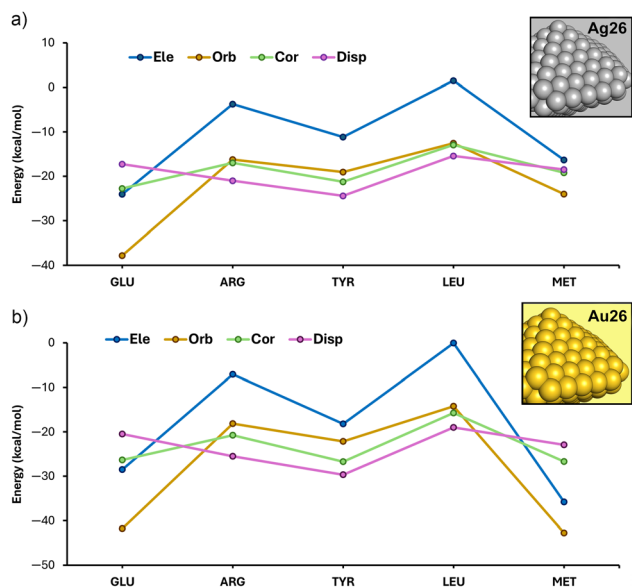
This journal is © the Owner Societies 2025

Phys. Chem. Chem. Phys., 2025, **27**, 9463–9469 | **9467**

Fig. 5 Graphical representation of the Ele, Orb, Cor and Disp terms for complexes **4** and **24** (LEU), **7** and **27** (TYR), **10** and **30** (GLU), **12** and **32** (ARG) and **14** and **34** (MET).

stability of these supramolecular assemblies. This behavior was also observed for their Au26 analogues (complexes **32**, **27** and **24**). Additionally, in the case of complexes involving GLU (**10**) and MET (**14**), the orbital contribution was the most favorable one, followed by electrostatics and correlation, which exhibited very similar values in the case of complex **10** involving GLU.

In the case of complex **14**, the dispersion term exhibited a close value to electrostatics and correlation, while for complex **10** it was the least favorable energy term. On the other hand, complex **30** involving GLU exhibited the same tendency as its Ag26 analogue (**10**), while in the case of complex **34** involving MET, electrostatics and dispersion terms inverted their behavior compared to complex **14**, with the latter being the least favorable energy contributor.

Conclusions

In conclusion, we have evaluated the stability and structural features of a series of AA···Ag/AuNP complexes at the PBE0-D3/def2-TZVP level of theory. The interaction energies were favourable in all the cases, ranging between -18.7 and -3.8 kcal mol^{-1} in the case of the Ag-involving complexes and between -27.6 and -5.7 kcal mol^{-1} in the case of the Au-involving complexes. The QTAIM and NCIplot analyses revealed that several NCIs (*e.g.* CH–Rg, RgB and Rg–π) are responsible for the molecular recognition phenomena between the AA and the NP, which has not been previously described in the literature. Lastly, the EDA analyses highlighted dispersion and orbital terms as the most prominent contributions in the overall stabilization of the AAs onto the Ag and Au metallic surfaces. The results reported in this exploratory study will be useful to account for the presence and physical nature of these weak bonds that ultimately regulate the AA···Ag/AuNP

recognition phenomena, a crucial molecular event related to the fields of bioinorganic chemistry, biotechnology and supramolecular chemistry.

Author contributions

C. N., S. B. and M. N. P. performed the theoretical calculations, and A. B. directed the study and wrote the article.

Data availability

Data for this article, including the cartesian coordinates of complexes **1–40**, are available in GitHub at **https://github.com/tonibr9/AA_NP.git**. Additionally, the ESI† contains Tables S1 and S2 and Fig. S1 and S2.

Conflicts of interest

There are no conflicts to declare.

Acknowledgements

References

1 (*a*) D. F. Emerich and C. G. Thanos, *Expert Opin. Biol. Ther.*, 2003, **3**, 655; (*b*) A. Haleem, M. Javaid, R. P. Singh, S. Rab and R. Suman, *Glob. J. Health Sci.*, 2023, **7**, 70; (*c*) S. Malik, K. Muhammad and Y. Waheed, *Molecules*, 2023, **28**, 6624.

2 (*a*) M. Manoharan, *Technol. Soc.*, 2008, **30**, 401; (*b*) Y. Hu and C. M. Niemeyer, *Adv. Mater.*, 2019, **31**, 1806294; (*c*) S. Talebian, T. Rodrigues, J. das Neves, B. Sarmento, R. Langer and J. Conde, *ACS Nano*, 2021, **15**, 15940.

3 (*a*) G. Perret, P. Ginet, M. C. Tarhan, A. Baccouche, T. Lacornerie, M. Kumemura, L. Jalabert, F. Cleri, E. F. Lartigau, B. J. Kim, S. L. Karsten, H. Fujita, Y. Rondelez, T. Fujii and D. Collard, *Solid-State Electron.*, 2016, **115**, 66; (*b*) M. Sarikaya, C. Tamerler, A. K.-Y. Jen, K. Schulten and F. Baneyx, *Nat. Mater.*, 2003, **2**, 577; (*c*) I. Y. Wong, S. N. Bhatia and M. Toner, *Genes Dev.*, 2013, **27**, 2397.

4 T. Shanmugasundaram, M. Radhakrishnan, V. Gopikrishnan, K. Kadirvelu and R. Balagurunathan, *Nanoscale*, 2017, **9**, 16773.

5 (*a*) P. Tan, H. Li, J. Wang and S. C. B. Gopinath, *Biotechnol. Appl. Biochem.*, 2020, **68**, 1236; (*b*) N. Ibrahim, N. D. Jamaluddin, L. L. Tan and N. Y. Mohd Yusof, *Sensors*, 2021, **21**, 5114; (*c*) F. Zeng, D. Xu, C. Zhan, C. Liang, W. Zhao, J. Zhang, H. Feng and X. Ma, *ACS Appl. Nano Mater.*, 2018, **1**, 2748; (*d*) P. Bollela, C. Schulz, G. Favero, F. Mazzei, R. Ludwig, L. Gorton and R. Antiochia, *Electroanalysis*, 2017, **29**, 77.

6 (*a*) S. Patra, S. Mukherjee, A. Kumar Barui, A. Ganguly, B. Sreedhar and C. R. Patra, *Mater. Sci. Eng. C*, 2015, **53**, 298; (*b*) M. Yamada, M. Foote and T. W. Prow, *WIREs*

9468 | *Phys. Chem. Chem. Phys.*, 2025, **27**, 9463–9469

This journal is © the Owner Societies 2025

Nanomed. Nanobiotechnol., 2015, **7**, 428; (*c*) R. S. Devi, A. Girigoswami, M. Siddharth and K. Girigoswami, *Appl. Biochem. Biotechnol.*, 2022, **194**, 4187.

7 (*a*) A. H. Pakiari and Z. Jamshidi, *J. Phys. Chem. A*, 2007, **111**, 4391; (*b*) N. S. AL-Thabaiti, M. A. Malik and Z. Khan, *Int. J. Biol. Macromol.*, 2017, **95**, 421; (*c*) H. Poblete, A. Agarwal, S. S. Thomas, C. Bohne, R. Ravichandran, J. Phopase, J. Comer and E. I. Alarcon, *Langmuir*, 2016, **32**, 265.

8 J. M. Slocik, M. O. Stone and R. R. Naik, *Small*, 2005, **1**, 1048.

9 Q. Zeng, X. Jiang, A. Yu and G. M. Lu, *Nanotechnology*, 2007, **18**, 035708.

10 Y. Li, Z. Tang, P. N. Prasad, M. R. Knecht and M. T. Swihart, *Nanoscale*, 2014, **6**, 3165.

11 (*a*) A. A. Shemetov, I. Nabiev and A. Sukhanova, *ACS Nano*, 2012, **6**, 4585; (*b*) Y. N. Tan, J. Y. Lee and D. I. C. Wang, *J. Am. Chem. Soc.*, 2010, **132**, 5677; (*c*) A. Vallee, V. Humblot and C.-M. Pradier, *Acc. Chem. Res.*, 2010, **43**, 1297.

12 (*a*) S. J. Park, *Int. J. Nanomed.*, 2020, 5783; (*b*) F. Pederzoli, G. Tosi, M. A. Vandelli, D. Belletti, F. Forni and B. Ruozi, *WIREs Nanomed. Nanobiotechnol.*, 2017, **9**, e1467.

13 J. M. Galloway and S. S. Staniland, *J. Mat. Chem.*, 2012, **22**, 12423.

14 (*a*) A. Kumar, X. Zhang and X.-J. Liang, *Biotechnol. Adv.*, 2013, **31**, 593; (*b*) F.-Y. Kong, J.-W. Zhang, R.-F. Li, Z.-X. Wang, W.-J. Wang and W. Wang, *Molecules*, 2017, **22**, 1445.

15 (*a*) I. P. Muhka, A. M. Eremenko, N. P. Smirnova, A. I. Mikhienkova, G. I. Korchak, V. F. Gorchev and A. Y. Chunikhin, *Appl. Biochem. Microbiol.*, 2013, **49**, 199; (*b*) N. Durán, G. Nakazato and A. B. Seabra, *Appl. Microbiol. Biotechnol.*, 2016, **100**, 6555; (*c*) C. Vanlalveni, S. Lallianrawna, A. Biswas, M. Selvaraj, B. Changmai and S. L. Rokhum, *RSC Adv.*, 2021, **11**, 2804.

16 Z. E. Hughes, L. B. Wright and T. R. Walsh, *Langmuir*, 2013, **29**, 13217.

17 J. P. Palafox-Hernandez, Z. Tang, Z. E. Hughes, Y. Li, M. T. Swihart, P. N. Prasad, T. R. Walsh and M. R. Knecht, *Chem. Mater.*, 2014, **26**, 4960.

18 C. Adamo and V. Barone, *J. Chem. Phys.*, 1999, **110**, 6158.

19 M. Ernzerhof and G. E. Scuseria, *J. Chem. Phys.*, 1999, **110**, 5029.

20 S. Grimme, J. Antony, S. Ehrlich and H. Krieg, *J. Chem. Phys.*, 2010, **132**, 154104.

21 A. Schäfer, H. Horn and R. Ahlrichs, *J. Chem. Phys.*, 1992, **97**, 2571.

22 S. G. Balasubramani, G. P. Chen, S. Coriani, M. Diedenhofen, M. S. Frank, Y. J. Franzke, F. Furche, R. Grotjahn, M. E. Harding, C. Hättig, A. Hellweg, B. Helmich-Paris, C. Holzer, U. Huniar, M. Kaupp, A. M. Khah, S. K. Khani, T. Müller, F. Mack, B. D. Nguyen, S. M. Parker, E. Perlt, D. Rappoport, K. Reiter, S. Roy, M. Rückert, G. Schmitz, M. Sierka, E. Tapavicza, D. P. Tew, C. van Wüllen, V. K. Voora, F. Weigend, A. Wodyński and J. M. Yu, *J. Chem. Phys.*, 2020, **152**, 184107.

23 K. Sawabe and A. Satsuma, *ACS Omega*, 2022, **7**, 4405.

24 A. Schäfer, A. Klamt, D. Sattel, J. C. W. Lohrenz and F. Eckert, *Phys. Chem. Chem. Phys.*, 2000, **2**, 2187.

25 M. J. Frisch, G. W. Trucks, H. B. Schlegel, G. E. Scuseria, M. A. Robb, J. R. Cheeseman, G. Scalmani, V. Barone, G. A. Petersson, H. Nakatsuji, X. Li, M. Caricato, A. V. Marenich, J. Bloino, B. G. Janesko, R. Gomperts, B. Mennucci, H. P. Hratchian, J. V. Ortiz, A. F. Izmaylov, J. L. Sonnenberg, D. Williams-Young, F. Ding, F. Lipparini, F. Egidi, J. Goings, B. Peng, A. Petrone, T. Henderson, D. Ranasinghe, V. G. Zakrzewski, J. Gao, N. Rega, G. Zheng, W. Liang, M. Hada, M. Ehara, K. Toyota, R. Fukuda, J. Hasegawa, M. Ishida, T. Nakajima, Y. Honda, O. Kitao, H. Nakai, T. Vreven, K. Throssell, J. A. MontgomeryJr., J. E. Peralta, F. Ogliaro, M. J. Bearpark, J. J. Heyd, E. N. Brothers, K. N. Kudin, V. N. Staroverov, T. A. Keith, R. Kobayashi, J. Normand, K. Raghavachari, A. P. Rendell, J. C. Burant, S. S. Iyengar, J. Tomasi, M. Cossi, J. M. Millam, M. Klene, C. Adamo, R. Cammi, J. W. Ochterski, R. L. Martin, K. Morokuma, O. Farkas, J. B. Foresman and D. J. Fox, Gaussian, Inc, Wallingford CT, 2016.

26 R. Dennington, T. A. Keith and J. M. Millam, *GaussView, Version 6*, Semichem Inc, Shawnee Mission, KS, USA, 2016.

27 R. F. W. Bader, *Chem. Rev.*, 1991, **91**, 893.

28 AIMAll (Version 19.10.12), T. A. Keith, TK Gristmill Software, Overland Park KS, USA, 2019.

29 L. Zhao and M. von Hopffgarten, *WIREs Comp. Rev.*, 2018, **8**, e1345.

30 K. Kitaura and K. Morokuma, *Int. J. Quantum Chem.*, 1976, **10**, 325.

31 J. Contreras-García, E. R. Johnson, S. Keinan, R. Chaudret, J.-P. Piquemal, D. N. Beratan and W. Yang, *J. Chem. Theory Comput.*, 2011, **7**, 625.

32 W. Humphrey, A. Dalke and K. Schulten, *J. Mol. Graphics*, 1996, **14**, 33.

33 M. N. Piña, J. Morey, A. Frontera and A. Bauzá, *J. Mater. Chem. A*, 2023, **11**, 25865.

34 J. H. Stenlid and T. Brinck, *J. Am. Chem. Soc.*, 2017, **139**, 11012.

35 J. H. Stenlid, A. J. Johansson and T. Brinck, *Phys. Chem. Chem. Phys.*, 2018, **20**, 2676.

36 I. Alkorta, J. Elguero and A. Frontera, *Crystals*, 2020, **10**, 180.

37 I. Alkorta, N. R. Walker and A. C. Legon, *Inorganics*, 2021, **9**, 13.

38 G. Sánchez-Sanz, C. Trujillo, I. Alkorta and J. Elguero, *Chem. Phys. Chem.*, 2019, **20**, 1552.

39 G. Sánchez-Sanz, C. Trujillo, I. Alkorta and J. Elguero, *Chem. Phys. Chem.*, 2020, **21**, 2557.

40 A. Frontera and A. Bauzá, *Chem. – Eur. J.*, 2018, **24**, 7228.

This journal is © the Owner Societies 2025

Phys. Chem. Chem. Phys., 2025, **27**, 9463–9469 | **9469**